JOURNAL OF GEOPHYSICAL RESEARCH, VOL. 111, D19207, doi:10.1029/2005JD007002, 2006

What determines altocumulus dissipation time?

Vincent E. Larson,[1] Adam J. Smith,[1] Michael J. Falk,[1] Kurt E. Kotenberg,[1] and Jean-Christophe Golaz[2]

Received 16 December 2005; revised 30 May 2006; accepted 26 June 2006; published 14 October 2006.

[1] This paper asks what factors influence the dissipation time of altocumulus clouds. The question is addressed using three-dimensional, large-eddy simulations of a thin, midlevel cloud that was observed by aircraft. The cloud might be aptly described as ''altostratocumulus'' because it was overcast and contained radiatively driven turbulence. The simulations are used to construct a budget equation of cloud water. This equation allows one to directly compare the four processes that diminish liquid: diffusional growth of ice crystals, large-scale subsidence, radiative heating, and turbulent mixing of dry air into the cloud. Various sensitivity studies are used to find the ''equivalent sensitivity'' of cloud decay time to changes in various parameters. A change from no sunlight to direct overhead sunlight decreases the lifetime of our simulated cloud as much as increasing subsidence by 1.2 cm s^{-1}, increasing ice number concentration by 780 m^{-3}, or decreasing above-cloud total water mixing ratio by 0.60 g kg^{-1}. Finally, interactions among the terms in the cloud water budget are summarized in a ''budget term feedback matrix.'' It is able to diagnose, for instance, that in our particular simulations, the diffusional growth of ice is a negative feedback.

Citation: Larson, V. E., A. J. Smith, M. J. Falk, K. E. Kotenberg, and J.-C. Golaz (2006), What determines altocumulus dissipation time?, *J. Geophys. Res.*, *111*, D19207, doi:10.1029/2005JD007002.

1. Introduction

[2] Altocumulus clouds are thin, turbulent cloud layers that occur at the midlevels of the troposphere [*Gedzelman*, 1988]. Study of these clouds is motivated by both practical and theoretical concerns. A practical motivation is that altocumuli often contain supercooled water, posing an icing hazard for small aircraft and unmanned aerial vehicles. A theoretical motivation is that altocumuli provide a simple laboratory with which to study the interaction of latent heating, microphysics, radiation, and turbulence.

[3] However, thin midlevel clouds are poorly predicted by current general circulation models (GCMs). *Zhang et al.* [2005] found that all GCMs in their intercomparison grossly underpredicted thin midlevel clouds, such as altocumuli, and overpredicted thick midlevel clouds, such as nimbostratus clouds. In related work, several authors have shown that large-scale models misrepresent thicker (frontal) midlevel clouds in various ways [e.g., *Katzfey and Ryan*, 2000; *Ryan et al.*, 2000; *Weaver et al.*, 2005; *Xu et al.*, 2005].

[4] Despite the desirability of greater understanding of altocumuli, they are less studied than other cloud types. For instance, a search on Science Citation Index yields over 1000 abstracts or titles containing the keyword ''cirrus'', roughly 1000 containing ''stratocumulus'', but less than 100 for ''altocumulus'' or ''altostratus'' or ''frontal cloud''. One could aptly call thin midlevel clouds the ''forgotten clouds'' [*Vonder Haar et al.*, 1997; *Fleishauer et al.*, 2002].

[5] In this article, we will investigate the time required by altocumuli to decay or dissipate. This depends on four main factors: precipitation, large-scale subsidence, radiative heating or cooling, and turbulent mixing with air outside the cloud. To investigate these factors, we will perform large-eddy simulations (LES) of an observed case. The case was an overcast cloud layer that decayed as it was observed by aircraft [*Larson et al.*, 2001].

[6] To analyze the causes of the decay in the simulations, we use several diagnostics that have received little or no application to altocumuli. First, we construct a horizontally averaged cloud water budget. This enables us to determine which of the four main processes listed above contribute most to depletion of liquid water. Second, we perform sensitivity studies, varying subsidence velocity, ice number concentration, solar zenith angle, and above-cloud moisture. The relative effectiveness of perturbations in these processes in changing cloud lifetime is encapsulated in ''equivalent sensitivities.'' Third, we examine how terms in the cloud water budget interact with one another. These feedbacks are summarized in a matrix that provides a convenient overview of how the four processes interact.

2. Case Background: 11 November Cloud

[7] The cloud we simulate was observed on 11 November 1999 during the fifth of the Complex Layered-Cloud Experiments (CLEX-5) [*Fleishauer et al.*, 2002]. It was a

[1] Atmospheric Science Group, Department of Mathematical Sciences, University of Wisconsin-Milwaukee, Milwaukee, Wisconsin, USA.

[2] University Corporation for Atmospheric Research Visiting Scientist Program, NOAA Geophysical Fluid Dynamics Laboratory, Princeton University, Princeton, New Jersey, USA.

0148-0227/06/2005JD007002$09.00

thin, mixed-phase layer cloud that was located between 5200 m and 5700 m MSL. The cloud top surface was fairly flat but had mounded elements created by radiatively driven turbulence. In the standard classification, a cloud with these properties would be categorized as altocumulus (see Glossary of Meteorology, http://amsglossary.allenpress.com), although the cloud was perhaps a bit thicker (500 m) than a typical altocumulus.

[8] However, we feel that the standard nomenclature is misleading for this cloud because it was overcast (i.e., had 100% cloud fraction). In common usage, when referring to the boundary layer, stratocumulus cloud layers denote nearly or entirely overcast layers, whereas cumulus cloud layers denote partly cloudy layers. By analogy, it would be more straightforward to denote overcast altocumulus layers ''altostratocumulus'' (which we abbreviate as ASc) and reserve the term ''altocumulus'' for partly cloudy altocumulus layers. *Kogan et al.* [2001] have used the term ''altostratocumulus'' previously, but the cloud so denoted was 5.5 km thick and had significant radar reflectivity at cloud base. For these reasons, we think their cloud would be better classified as ''altostratus'' or ''nimbostratus.''

3. Aircraft Data

[9] The observations we use were obtained by aircraft-borne instruments that are described by *Fleishauer et al.* [2002] and *Poellot et al.* [1999]. To analyze liquid water, we use King Probe data, suitably corrected for offset errors. To measure ice concentration and mixing ratio, we use a 2D-C probe, which measures particles from 33 to 1056 microns in diameter [*Fleishauer et al.*, 2002]. One shortcoming of the experiment was that it lacked a 2D-P probe to measure larger ice crystals. A Cloud Particle Imager (CPI) was used to obtain detailed pictures of individual ice crystals, but the data were not suitable for obtaining accurate number concentrations. However, the CPI did photograph some ice crystals larger than 1000 microns.

4. Numerical Model

[10] The numerical model we use is the Coupled Ocean/Atmosphere Mesoscale Prediction System (COAMPS®) Large-Eddy Simulation (COAMPS-LES) model [*Golaz et al.*, 2005]. COAMPS-LES model output has compared well with results from several intercomparisons of boundary layer cumulus and stratocumulus layers organized by Global Energy and Water Experiment (GEWEX) Cloud System Study (GCSS) [e.g., *Brown et al.*, 2002; *Stevens et al.*, 2001, 2005; *Golaz et al.*, 2005].

[11] Our simulations are 3D, high-resolution LES. We are not aware of previous altostratocumulus simulations of this type. However, several 2D LES of ASc have been performed [*Starr and Cox*, 1985; *Liu*, 1998; *Liu and Krueger*, 1998; *Clark et al.*, 2005] and several coarser-resolution 3D cloud resolving simulations of frontal clouds have been performed [*Ryan et al.*, 2000; *Katzfey and Ryan*, 2000; *Xu et al.*, 2005; *Weaver et al.*, 2005].

[12] In COAMPS-LES, the prognostic variables are the Cartesian wind components, dry potential temperature (θ), and water vapor (r_v) and cloud water (r_c) mixing ratios. The perturbation pressure is computed using a recently introduced anelastic option. The momentum variables are advected by a second-order advection scheme, and the scalars are advected by a positive definite advection scheme with second-order polynomial interpolation [*Bott*, 1989]. We use a TKE subgrid scale option [*Deardorff*, 1980].

[13] The simulations we present were run with a grid spacing of 50 m $\times$ 50 m in the horizontal and 15 m in the vertical. To save computational expense, the bottom of the domain was placed in the midtroposphere, with zero momentum and thermodynamic fluxes applied at the lower boundary. The domain size was chosen to be 2400 m in the vertical and 4050 m $\times$ 4050 m in the horizontal. The time step was set to 1 s. We performed a simulation in which the grid spacing was halved in all directions, but the results were nearly the same, with an increase in cloud lifetime of only 12 min.

[14] The 11 November case had little vertical wind shear. We chose the initial horizontal wind profile to be zero, and in doing so lost no generality, because the cloud system was Galilean invariant. Furthermore, the flight pattern was Lagrangian; that is, the aircraft remained within the same column of air as the column drifted horizontally with the wind [*Fleishauer et al.*, 2002]. Therefore we need not impose a forcing due to horizontal advection of thermodynamic scalars and momentum. Also, the Coriolis parameter was set to zero because the simulations are brief. We imposed large-scale subsidence by choosing a constant subsidence velocity and using it to vertically advect the prognostic scalars (liquid, vapor, and potential temperature) and the horizontal components of wind.

4.1. Radiative Transfer Scheme

[15] Turbulence in layer clouds is driven partly by radiative cooling near cloud top and radiative heating near cloud base. Direct numerical radiative computations are expensive, particularly for midlevel clouds, which exchange radiation with the ground, which is far below cloud base. Instead we use idealized approximations. Our radiative transfer calculations include the effects of liquid but not ice, because the observed mixing ratio of ice is much smaller than that of liquid [*Fleishauer et al.*, 2002]. We assume a droplet effective radius of 10 microns. On the basis of observations, we use a ground surface temperature and albedo of 287 K and 0.1 respectively. We compute shortwave radiation using the two-stream, single-band model of *Shettle and Weinman* [1970] (see also *Duynkerke et al.* [2004]). We approximate the net vertical longwave radiative flux at altitude z, $F(z)$, following *Stevens et al.* [2005]

$$F(z) = F_0 \exp[-\kappa LWP(z)] + F_1 \exp\{-\kappa[LWP(0) - LWP(z)]\}, \quad (1)$$

where the liquid water path, $LWP(z)$, from the top of the atmosphere to the altitude z is given by

$$LWP(z) = \int_z^\infty \rho r_c dz'. \quad (2)$$

Here ρ is air density and r_c is cloud water mixing ratio. We choose $F_0 = 104\ \mathrm{W\,m^{-2}}$, $F_1 = 62\ \mathrm{W\,m^{-2}}$, and $\kappa = 94.2\ \mathrm{m^2\,kg^{-1}}$

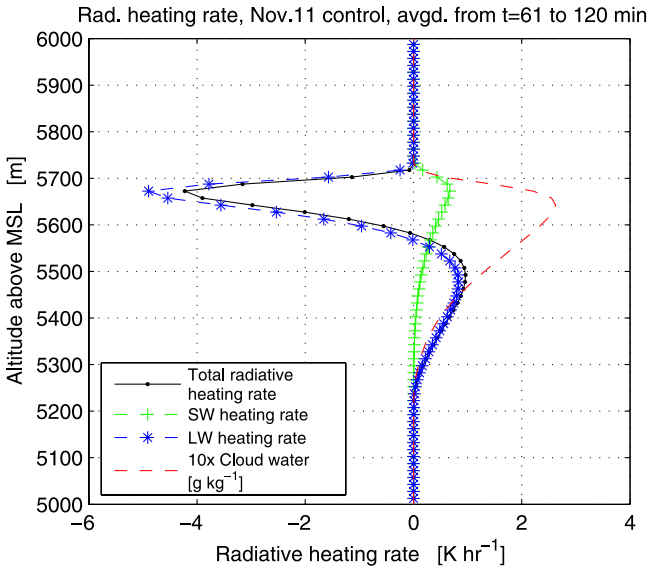

Figure 1. Profile of total (line with dots), shortwave (pluses), and longwave (asterisks) radiative heating rate averaged over the first simulated hour after spin-up. For reference, we also plot the cloud water profile (dashed line) averaged over the same time period. There is net radiative cooling near cloud top and net radiative heating near cloud base. Compared with stratocumulus, the cloud base heating is stronger because the temperature differential between ground and cloud base is larger.

on the basis of extensive comparison [*Larson et al.*, 2006] with a sophisticated two-stream numerical radiative transfer code, BUGSrad [*Stephens et al.*, 2001, 2004]. These values lead to significant cloud top cooling, due to radiant energy lost to space, and also significant cloud base warming, due to radiant energy received from the ground (see Figure 1). Compared to stratocumulus, the cloud base warming in altostratocumulus is much more prominent, because there is a greater temperature difference between cloud base and the ground far below. In fact, the vertically integrated cloud base warming is only moderately less than the vertically integrated cloud top cooling.

4.2. Ice Microphysics Scheme

[16] In a mixed-phase cloud, liquid water is depleted as ice crystals grow by vapor diffusion (the Bergeron-Findeisen process) and by accretion of supercooled droplets. CPI images [*Fleishauer et al.*, 2002] indicate that although some accretion did occur in the 11 November cloud, diffusional growth was more important. For this reason, we neglected accretion and implemented a model of ice diffusional growth based on the work of *Mitchell* [1996]. In general, ice crystals are thought to nucleate preferentially at cold temperatures [*Rogers and Yau*, 1989]. For simplicity, we assume that ice crystals nucleate only at cloud top, and that each newly nucleated crystal has a mass of $m = 10^{-11}$ kg. The number concentration of ice crystals in the control case ($N_i = 2000$ m^{-3}) is specified as the average concentration observed in legs near cloud base while the cloud was robust (legs 2 and 7) [*Fleishauer et al.*, 2002].

[17] Each crystal then grows according to the ice diffusional (depositional) growth equation [e.g., *Rogers and Yau*, 1989]:

$$\frac{dm}{dt} = G(T,p)4\pi C(S_i - 1), \tag{3}$$

where $G(T, p)$ is a slowly varying function of temperature T and pressure p, C is the ice capacitance, S_i is the saturation ratio with respect to ice, and t denotes time. The saturation ratio is approximated as $S_i = e_s/e_i$, where e_s and e_i are the saturation vapor pressures over liquid water and ice respectively. The crystal habit is specified as broad-branched plates, type P1c [*Pruppacher and Klett*, 1997], on the basis of CPI images. The capacitance C of ice crystals is approximated as that appropriate for plates, $C = D/\pi$ where D is the diameter of an ice crystal. The mass m and diameter of ice crystals are related by *Mitchell* [1996]:

$$m = a\left(\frac{D}{1\text{ m}}\right)^b, \tag{4}$$

where $a = 2.05 \times 10^{-3}$ kg and $b = 1.8$.

[18] As each crystal grows, it falls downward. The terminal velocity v_T, air density ρ, and diameter are related by

$$v_T = k_u\left(\frac{\rho}{1\text{ kg m}^{-3}}\right)^{-q}\left(\frac{D}{1\text{ m}}\right)^n, \tag{5}$$

where $k_u = 55$ m s^{-1}, $q = 0.17$, and $n = 0.70$. The simulated ice crystals are not advected by air motions. At each altitude, there is negligible horizontal variation in simulated ice particle size and ice water content. We neglect ice deposition and sublimation below cloud because these processes are unlikely to have an overriding effect on cloud lifetime. Since the CPI images showed very few drizzle drops, our simulations neglect drizzle processes. The ice processes cannot be well constrained by our observations, because the instrumentation did not include a 2D-P probe for larger ice crystals, and because the aircraft sampling was necessarily sparse. Sensitivity to changes in the microphysics scheme can be partly inferred by changing ice number concentration (see results below).

[19] Clearly, such an ice microphysics scheme is highly idealized. In particular, it omits three processes that may be of importance. First, the lack of ice advection prevents ice from being recycled from below cloud back into the cloud itself [*Köhler*, 1999]. Recycling is possible because the turbulence velocity scale is of the same order of magnitude as the terminal velocity. Second, the quasi-monodisperse distribution of ice precludes the possibility of a small number of ice crystals growing fortuitously to large sizes [*Gu and Liou*, 2000]. Third, the lack of sublimation below cloud base omits a source of cooling there [*Gu and Liou*, 2000].

[20] In order to partially address these omissions, we have rerun the control simulation using COAMPS' default microphysics scheme [*Hodur*, 1997], which is an updated version of that of *Rutledge and Hobbs* [1983]. This microphysics scheme is a bulk single-moment scheme with

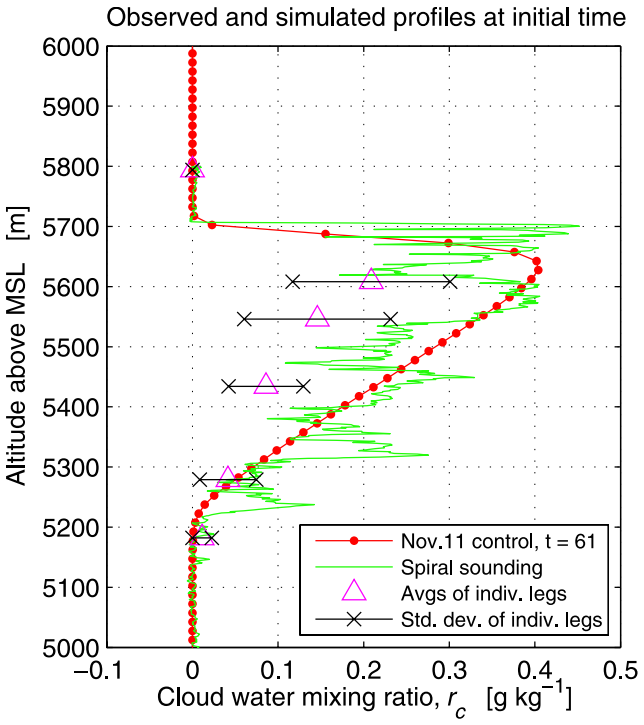

Figure 2. Profiles of observed cloud water mixing ratio r_c from an aircraft spiral sounding (solid line) and the simulation at the initial time after spin-up (line with dots) and from later aircraft legs (triangles). The distance between a cross and a triangle is one standard deviation. The simulated profile agrees well with the aircraft sounding; the aircraft legs were measured later, when the cloud had already dissipated somewhat.

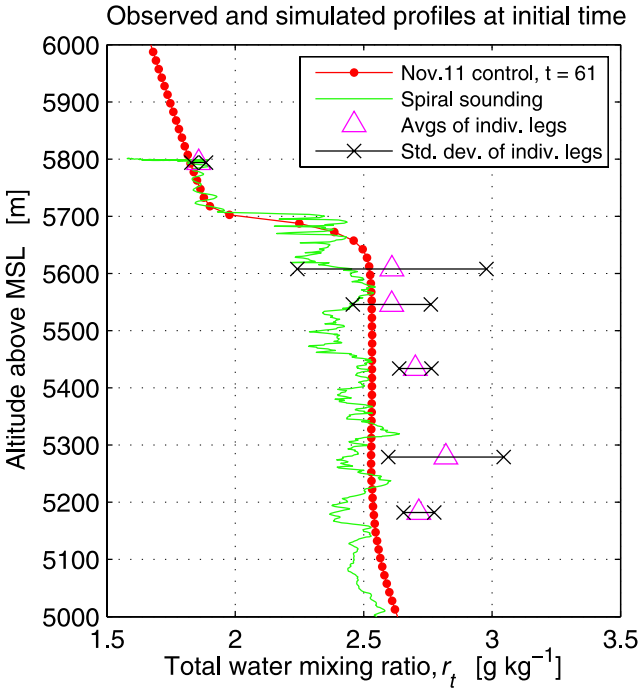

Figure 3. Same as Figure 2 except for total (vapor plus cloud) water mixing ratio r_t.

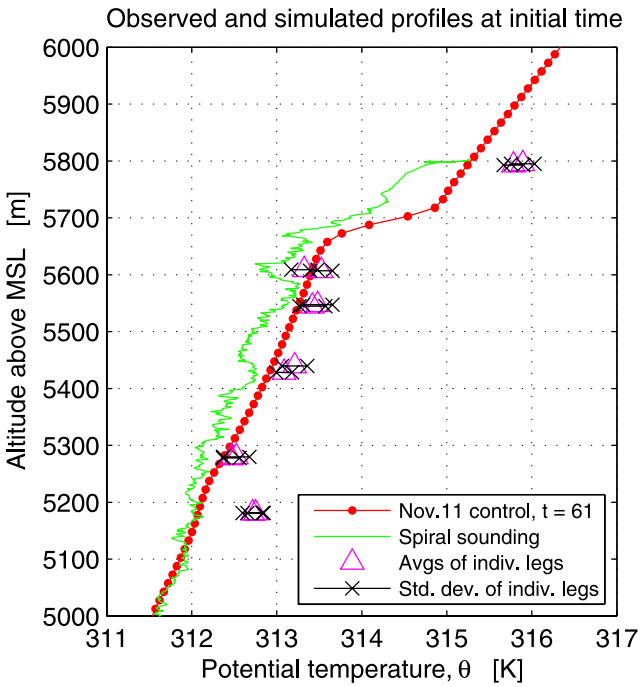

Figure 4. Same as Figure 2 except for potential temperature θ.

pristine ice and snow ice hydrometeor types. With this microphysics scheme, COAMPS advects ice in the horizontal and vertical, has a Marshall-Palmer size distribution of ice, and sublimates ice in subsaturated air. This microphysics scheme produces negligible sublimation cooling below cloud, and very similar cloud evolution and cloud lifetime to the idealized scheme (see section 5). This lends confidence in the idealized scheme.

[21] For this initial study, we choose to use the idealized microphysics scheme because its behavior is easy to interpret, and it is easy to implement in other models. The ease of implementation is useful for intercomparing model dynamics.

5. Comparison of the Control Simulation With Aircraft Data

[22] We now ask whether or not our control simulation resembles available aircraft data. The setup of our control simulation has an imposed large-scale subsidence rate of 3 cm s^{-1}, based on a short-term forecast from a high-resolution numerical weather model, MM5 [*Larson et al.*, 2001]. We set the cosine of the solar zenith angle to a constant value of 0.4329, as appropriate for the location and time of day of the observations. We choose the number concentration of ice crystals to be 2000 m^{-3}, as observed on the aircraft legs 2 and 7.

[23] First we display profiles of cloud water mixing ratio r_c (Figure 2), total water mixing ratio (vapor + liquid) r_t (Figure 3), potential temperature θ (Figure 4), and liquid water potential temperature θ_l (Figure 5). The solid lines correspond to an aircraft sounding taken at the beginning of the measurement period. The dotted lines correspond to horizontally averaged simulated "initial" profiles after a 1-hour spin-up period that enabled turbulence to equili-

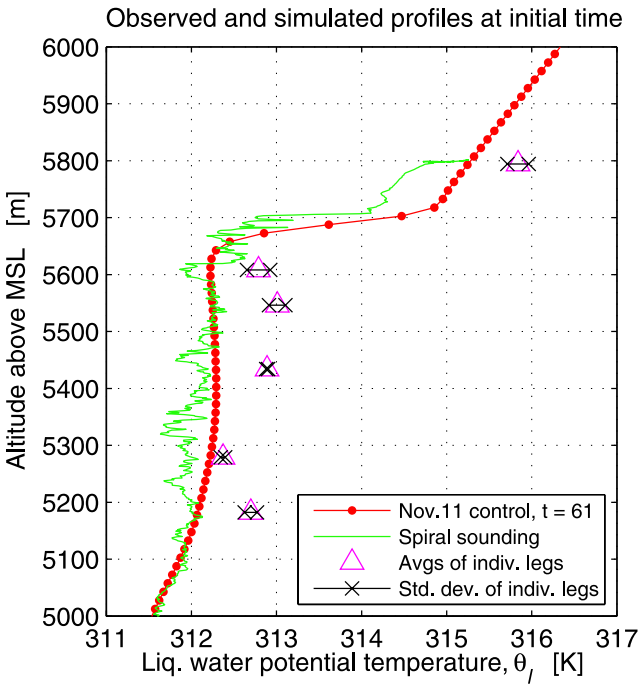

Figure 5. Same as Figure 2 except for liquid water potential temperature θ_l.

brate. The simulations have been set up so that these two sets of lines match as closely as possible. The simulated profiles are smoother because of horizontal averaging over the model domain. The noise in the observed soundings is partly an indication of horizontal variability. The triangles denote averages from horizontal aircraft legs that occurred later in the observation period; the distance between two crosses corresponds to two standard deviations. The triangles are displaced slightly from the aircraft soundings because of time evolution of the cloud.

[24] Cloud water r_c turns out to have a nearly adiabatic profile. Because r_t and θ_l are conserved variables in the absence of precipitation and radiative heating, they have profiles that are constant with altitude ("well-mixed profiles") in the presence of strong turbulence. In our simulations, total water r_t is well mixed in the vertical. However, θ_l is not completely well mixed, with slightly warmer values at cloud base than cloud top. Such a θ_l profile also occurs in simulations of boundary layer stratocumulus without cloud base heating. It occurs because the simulated turbulence has not completely mixed out the unstable profile that radiation attempts to produce.

[25] Given the available data, we may test the fidelity of the simulations in two ways. First, we compare the standard deviation of vertical velocity during the first hour after spin-up with observations (Figure 6). The simulated values are lower than observed, but still reasonable. Second, we compare the cloud lifetime from the beginning of aircraft observations until its final disappearance (top plot of Figure 7). The observed lifetime was 1 hour 14 min, whereas the simulated lifetime is 2 hours after spin-up, a difference of 46 min. However, in its last 25 min, the simulated cloud contained little cloud water ($r_c \leq 0.05$ g kg^{-1}). This is acceptable agreement, considering the idealizations in the simulations and uncertainties in the observations. Although the lifetime was measured accurately, the initial sounding may have been unrepresentative because of variability in the horizontal. One can estimate the effect of starting with a drier profile by regarding the beginning point in Figure 7 as being later than 61 min. Other uncertainties are the subsidence velocity and the above-cloud vapor mixing ratio.

[26] For comparison, a simulation that uses COAMPS' default ice microphysics scheme but is otherwise identical to the control case (Figure 7, top), is presented in the bottom plot of Figure 7. The difference in cloud lifetime is less than 10 min. This suggests that our idealized ice microphysics scheme produces plausible results.

6. Budgets for the Control Simulation

[27] What physical processes contribute most to changes in moisture and temperature? This question is addressed by budget equations [e.g., *Stull*, 1988].

6.1. Budget of Total Water Mixing Ratio

[28] The budget for total water mixing ratio r_t is listed in equation (A6) and shown in Figure 8. The plotted budget has been integrated in time in order to show how much various terms change r_t during the first hour after spin-up. Plotted for reference is the profile of cloud water r_c at the initial time, $t = 61$ min (dashed line). The heavy solid line is the total simulated change in r_t, that is, the r_t tendency integrated over the first hour. The tendency is nonpositive everywhere, which shows that r_t decreases or remains constant over time at all altitudes.

[29] What contributes to this decrease? At all altitudes within cloud, r_t is significantly depleted by diffusional

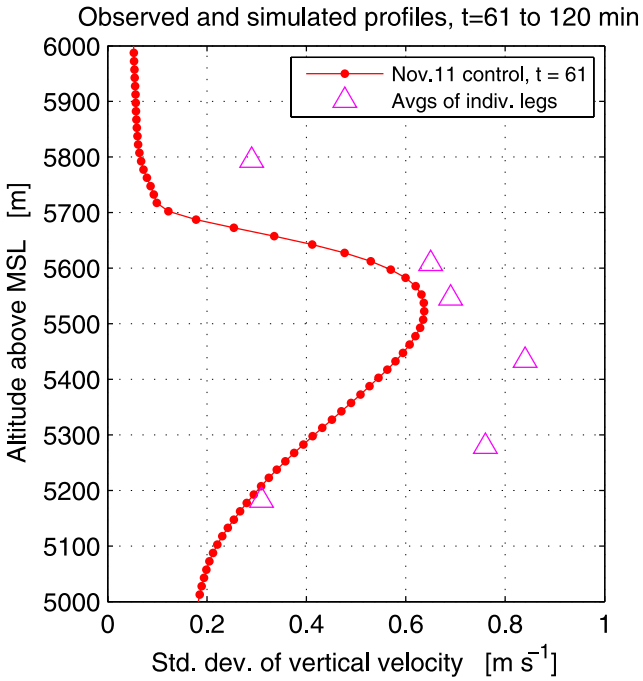

Figure 6. Standard deviation of vertical velocity as measured during horizontal aircraft legs (triangles) and as simulated over the first hour after spin-up (line with dots). The simulation generates a plausible magnitude of turbulence.

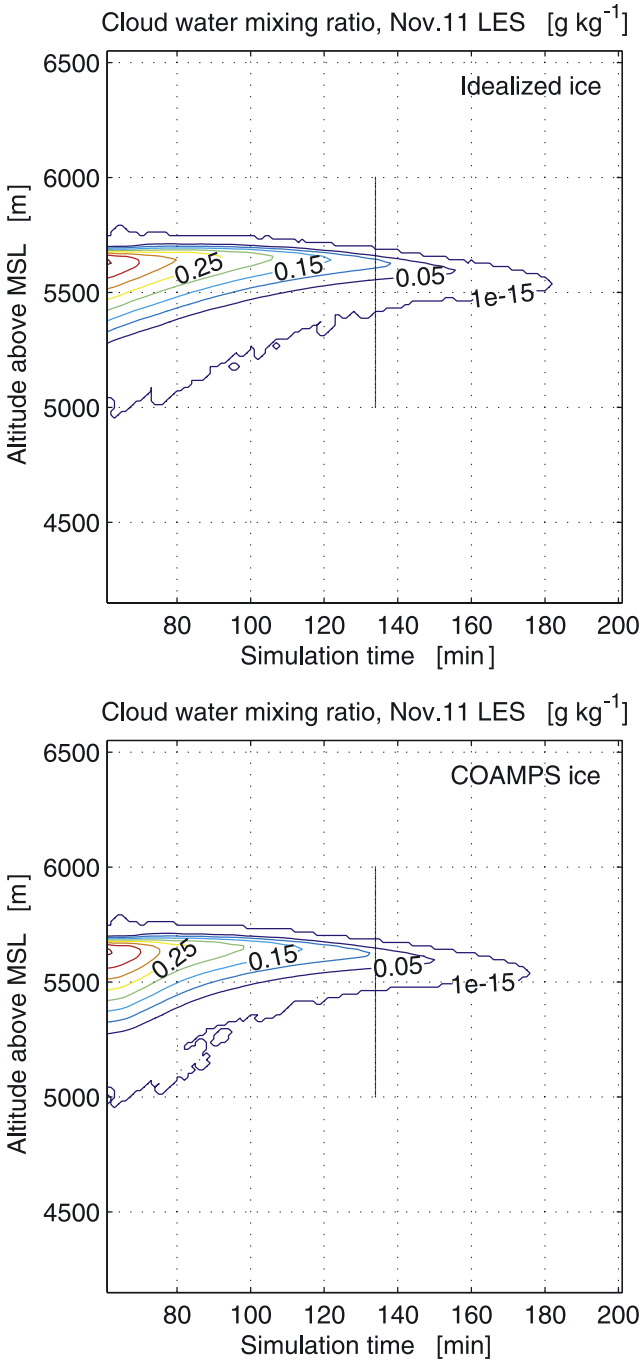

Figure 7. (top) Time-height slice of cloud water mixing ratio r_c beginning after the spin-up period ends at 60 min. The simulation uses our idealized microphysics for diffusional growth of ice. The simulated cloud disappears somewhat later (at t = 180 min) than the observed cloud (at t = 134 min, marked by vertical line). However, the simulated cloud water mixing ratio is very low in the last 25 min of the simulated cloud's life. (bottom) Same as the top plot but using COAMPS' bulk single-moment ice microphysics scheme. The results are similar, lending confidence in the idealized scheme.

growth of ice and its subsequent fallout (Figure 8, crosses). Subsidence (diamonds), $-\overline{w}\partial\overline{r_t}/\partial z$, has a strong drying effect (i.e., negative sign) near cloud top, where r_t falls off sharply with increasing height. The main effect of turbulent mixing (circles) is to remove r_t from within cloud and deposit it near the cloud top region. Turbulent mixing cannot be a net source or sink of r_t; that is, the mass-weighted vertical integral of turbulent mixing of r_t (circles) must be zero. The condensation/evaporation (triangles) of total water vanishes, as expected, since a gain of liquid accompanies an equal loss of vapor, and vice versa. This line is included as a test of the numerics, which in principle can have nonconservative transfers between vapor and liquid prognostic variables. Subgrid turbulent mixing (squares) is small, indicating that the cloud layer is well resolved. Other minor terms, related to numerical artifacts, are not displayed. The main message from the r_t budget is that ice diffusional growth and subsidence strongly dry the layer, but that turbulent mixing has a weaker net effect on the cloud, since it mainly redistributes r_t within cloud.

6.2. Budget of Liquid Water Potential Temperature

[30] Next we examine the budget of liquid water potential temperature, $\theta_l \cong \theta - r_c\,(L/c_p)\,(p_0/p)^{R_d/c_p}$ (Figure 9 and equation (A5)). Here L is the latent heat of vaporization, c_p is the specific heat of dry air at constant pressure, R_d is the gas constant for dry air, p is pressure, and p_0 is a reference pressure (1000 hPa). Our approximation of θ_l neglects ice because ice mixing ratio is small. Recall that θ_l is a conserved variable in the absence of precipitation and radiation. The variable θ_l reduces to θ in the absence of liquid. The total tendency of θ_l is nonnegative everywhere during the first simulated hour. Subsidence (diamonds), $-\overline{w}\partial\overline{\theta_l}/\partial z$, tends to heat the cloud top region, because of the temperature inversion there (see Figure 4). Ice diffusional growth (crosses) increases θ_l because it removes r_c. Radiation (stars) strongly heats cloud base and cools near cloud top, as expected from Figure 1. Turbulent mixing (circles) counteracts the net effect of the other terms, removing θ_l near cloud base and cloud top, and depositing it just below cloud top. Hence turbulent mixing renders the total θ_l tendency more uniform with height. The main message is similar to that for the r_t budget: subsidence and ice diffusional growth strongly heat the layer, and radiation and turbulent mixing do not have the same sign at all altitudes.

6.3. "Raw" Cloud Water Budget

[31] Budgets of r_t and θ_l are instructive because these variables are approximately conserved for the 11 November cloud (even though they neglect ice). To address the question of cloud lifetime, however, it is useful to examine a budget of cloud water. (We prefer cloud water as an indicator of cloud because it does not sediment rapidly, as does ice.) A budget of cloud water is shown in Figure 10. We call this a "raw" budget because each of its terms corresponds directly to a piece of code in the COAMPS-LES model. The raw budget contains terms similar to those in the r_t and θ_l budgets.

[32] The raw budget has several advantages. First, the raw budget terms correspond directly to terms computed by COAMPS-LES. Second, although COAMPS-LES contains

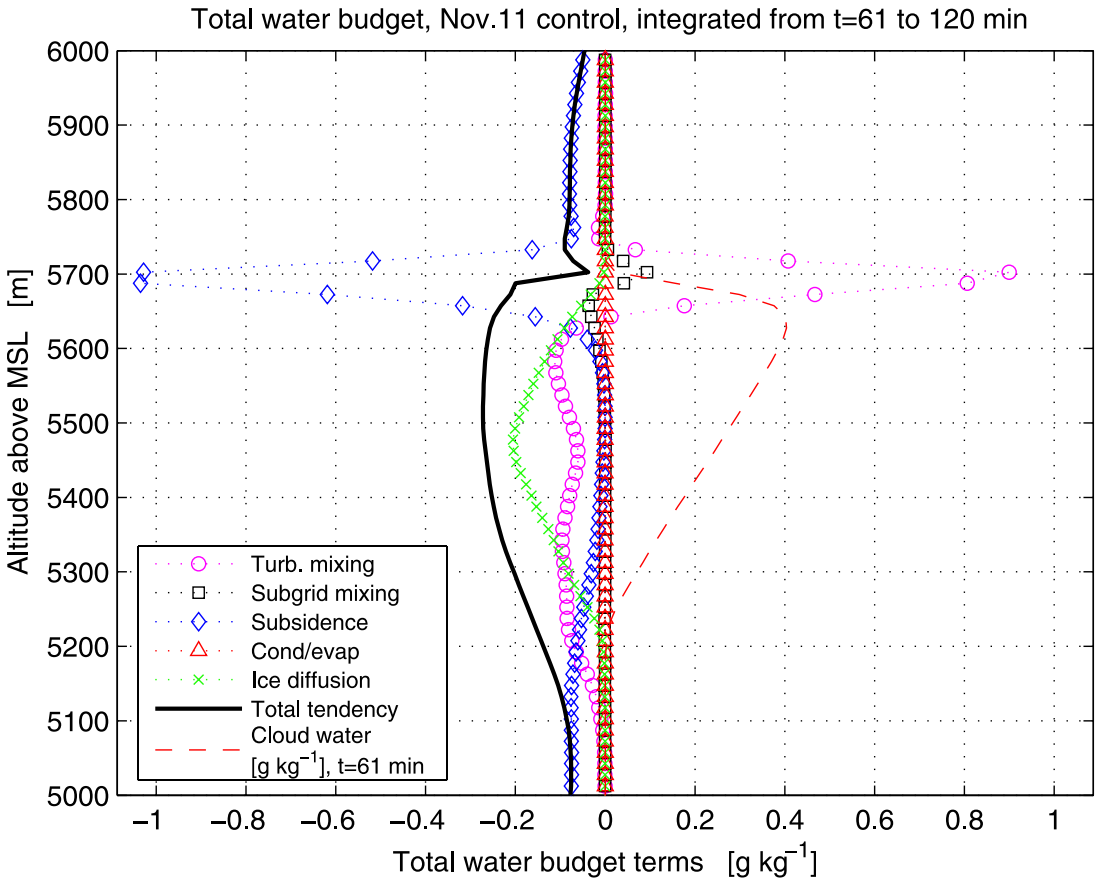

Figure 8. Budget of total water mixing ratio r_t, integrated over the first simulated hour after spin-up. For reference, we plot the cloud water mixing ratio (r_c) profile at the beginning of the hour (dashed line). The total tendency (solid line) is negative, implying net drying, with negative (drying) contributions from diffusional growth of ice (crosses) and large-scale subsidence (diamonds). Turbulent mixing (circles) removes r_t from low levels and deposits it near cloud top. Subgrid turbulent mixing (squares) is small except near cloud top. The condensation/evaporation term (triangles) is small, as appropriate for a conserved variable.

approximations, as do all LES models, the raw budget records COAMPS-LES output without introducing further approximations. In particular, unlike the budget based on conserved variables that we recommend below, the raw budget can account for supersaturated parcels, subsaturated parcels containing liquid, and horizontal layers that are partly cloudy. Therefore the raw budget provides a benchmark for other possible budgets, in particular, the budget that we recommend below.

[33] However, for our purposes, the raw budget has several drawbacks. The major problem is that the condensation/evaporation term (triangles) is large but is not attributed to specific physical processes, such as radiation, subsidence, etc. This prevents us from assessing the relative importance of all terms. Second, and relatedly, the budget contains no explicit radiation term. Third, the subsidence term (diamonds) does not incorporate all effects of subsidence. By this we mean the following. Cloud water at most altitudes in the 11 November case increases nearly adiabatically with increasing altitude. Subsidence brings down larger values of cloud water, thereby increasing r_c. However, subsidence also induces compressional heating and evaporation, thereby decreasing r_c. In an adiabatic cloud, these two effects cancel, leaving zero net effect on r_c. However, in the raw cloud water budget, the subsidence term is defined as $-\overline{w}\partial\overline{r_c}/\partial z$, which is positive in most regions of the cloud (diamonds in Figure 10), and which does not include evaporation. Rather, evaporation induced by subsidence is included in the condensation/evaporation term. This is not wrong, but it seems inconvenient to us.

6.4. Budget of Cloud Water Based on Conserved Variables

[34] To overcome these drawbacks, we have derived a new cloud water budget. The starting point of the derivation is the budgets of the conserved variables r_t and θ_l. These budgets are combined, along with the assumptions that there exists no supersaturation, nor subsaturation in the presence of liquid, in order to form a budget of cloud water (see Appendix A, especially equation (A4)). This cloud water budget is only valid when the cloud fraction is 0 or 1. This is adequate for our cloud because it is overcast and its cloud top is fairly flat. The cloud water budget based on conserved variables is presented in Figure 11. We have verified that, as desired, the integrated tendency of r_c (solid line) is nearly identical to both the simulated temporal change in r_c (not

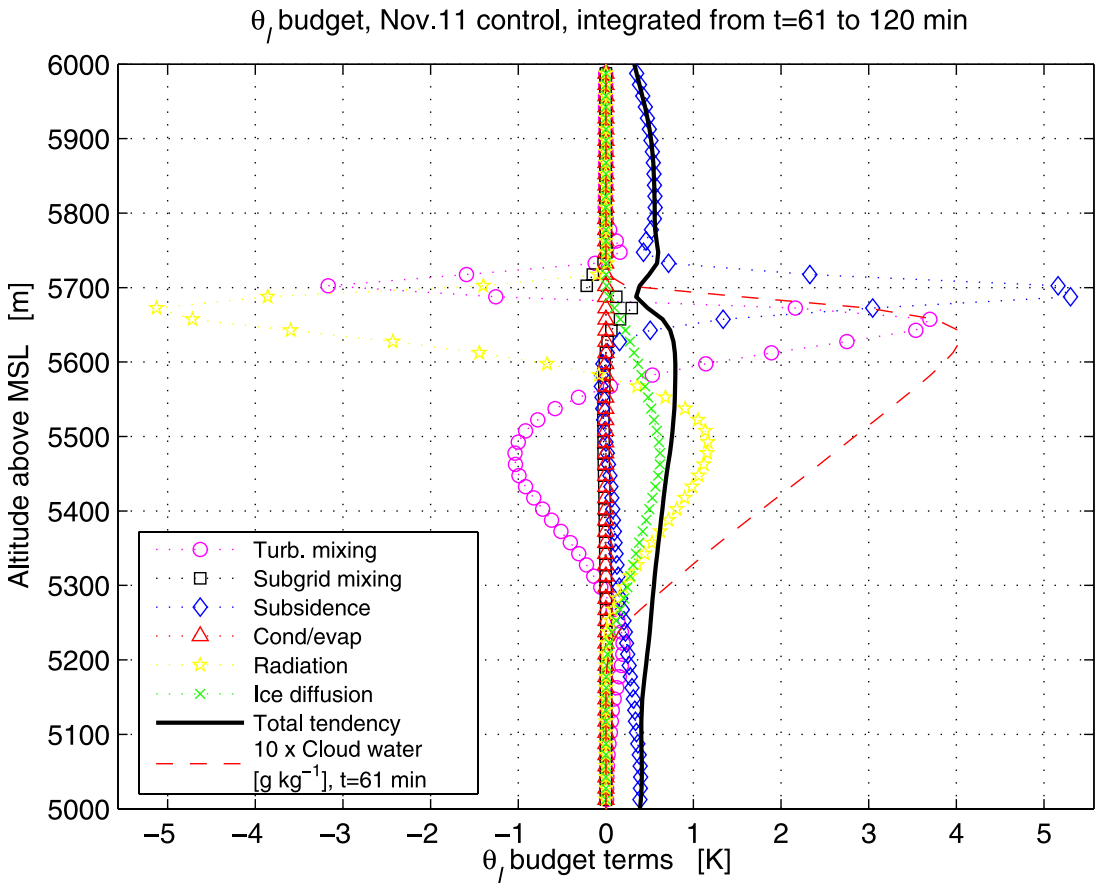

Figure 9. Budget of liquid water potential temperature θ_l, integrated over the first simulated hour after spin-up. For reference, we plot the cloud water mixing ratio (r_c) profile at the beginning of the hour (dashed line). The total tendency (solid line) is positive, implying net heating/drying, with positive contributions from diffusional growth of ice (crosses) and large-scale subsidence (diamonds). Radiation (stars) heats near cloud base and cools near cloud top, as seen also in Figure 1. Turbulent mixing (circles) removes θ_l from midlevels and deposits it above and below. Subgrid turbulent mixing (squares) is small except near cloud top. The condensation/evaporation term (triangles) is small, as appropriate for a conserved variable.

shown), and the integrated raw cloud water tendency (Figure 10).

[35] The "conserved" budget is easier to interpret than the raw budget. The condensation/evaporation term now vanishes (triangles) because it has been partitioned among other terms. The budget now includes a radiation term (stars), which depletes liquid near cloud base, where radiative heating occurs, and augments liquid near cloud top, where radiative cooling occurs, as expected. Depletion of liquid by subsidence (diamonds) now vanishes in the adiabatic parts of clouds, but is still strong near cloud top, as expected. This subsidence term can now be interpreted as the subsidence of the deviation from adiabaticity. The ice diffusion term (crosses) is the same as in the raw cloud water budget (Figure 10).

[36] Inspection of Figure 11 allows us to determine which physical processes deplete cloud water most strongly. Strong, single-signed, negative contributions are made by both ice diffusional growth and subsidence. In contrast, the radiation (stars) and turbulent mixing terms (circles) have different signs at different altitudes. Turbulent mixing tends to counterbalance the other terms and is a distorted mirror image of the turbulent mixing term in the θ_l budget.

[37] Our "conserved" cloud water budget differs from that of *Wang and Wang* [1999]. The chief advantage of their budget is that it applies to a partly cloudy layer, if its probability density function (PDF) is Gaussian. A difference is that their subsidence and turbulent mixing terms are the same as in our "raw" cloud water budget. The budget of *Wang and Wang* [1999] has not been applied to three-dimensional LES output, to our knowledge.

[38] Our budget also differs from that of *Wang et al.* [2003]. The advantage of this latter budget is that it permits supersaturation and also permits liquid in the presence of subsaturation. A disadvantage is that the condensation/evaporation term is not partitioned into contributions due to radiation, subsidence, etc.

6.5. How Our Budgets Include Entrainment

[39] It may appear at first that our budgets omit an important process, namely, cloud top entrainment. The cloud top entrainment velocity is the volume of fluid per

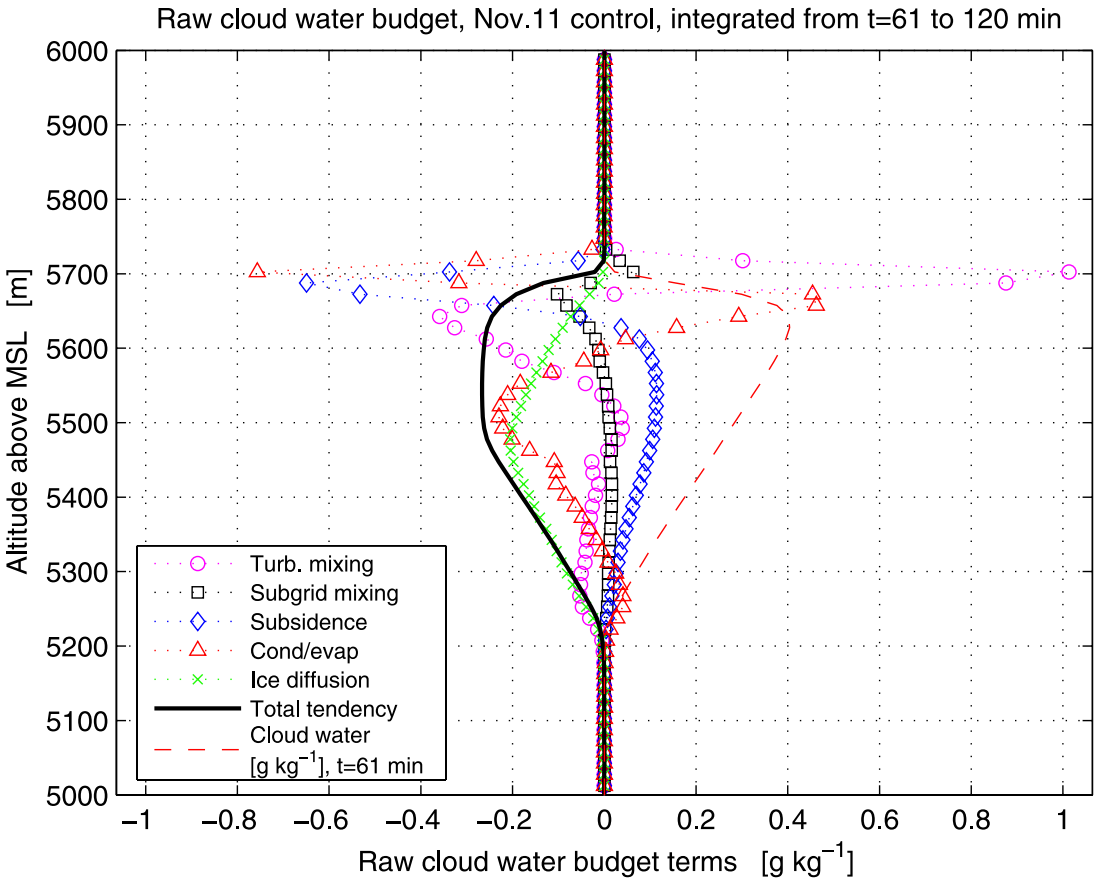

Figure 10. "Raw" budget of cloud water mixing ratio r_c, extracted directly from the LES code. The budget is integrated over the first simulated hour after spin-up. For reference, we plot the cloud water mixing ratio (r_c) profile at the beginning of the hour (dashed line). The total tendency (solid line) is negative, implying net depletion of cloud water. There is a negative (depleting) contribution from diffusional growth of ice (crosses). Large-scale subsidence (diamonds) depletes cloud water near cloud top but increases it below. Turbulent mixing (circles) has a complicated profile. Subgrid turbulent mixing (squares) is small except near cloud top. The condensation/evaporation term (triangles) is large, and its source is undetermined by this budget. The budget does not have an explicit radiation term.

unit area per time incorporated through cloud top from above. It can be estimated, for instance, by the rate of rise of cloud top with respect to large-scale vertical velocity. In our budget, entrainment is included in the turbulent mixing term. We prefer to analyze turbulent mixing rather than entrainment for several reasons.

[40] First, although it is easy to define entrainment velocity loosely (see above definition), it is more difficult to provide a practical, quantitative, and precise definition. For instance, cloud top is never perfectly flat and horizontal; rather, it contains time-dependent undulations due to turbulence. Also, although cloud top entrainment proceeds mainly in one direction (from above cloud into cloud), some cloudy air is detrained to the overlying air. In contrast, the turbulent mixing term can be derived mathematically and does not require the above idealizations.

[41] Second, turbulent mixing is more general than cloud top entrainment. For instance, turbulent mixing includes entrainment into cloud base from below. In well-mixed stratocumulus-topped boundary layers, cloud base entrainment is unimportant because the total water mixing ratio r_t below cloud equals that within cloud. In the 11 November ASc case, however, cloud base entrainment actually leads to moistening of the (upper part of) cloud; that is, it incorporates air with greater r_t (see Figure 8).

[42] Third, the turbulent mixing term provides a vertical profile of information, not merely a vertical integral. In particular, mixing describes how liquid is transported within cloud. This is necessary in order to create a budget that balances at every vertical level.

7. Sensitivity Study on Cloud Lifetime

[43] Recall that in the control simulation, we set the imposed subsidence velocity to w_s = 3 cm s^{-1}, the ice number concentration to N_i = 2000 m^{-3}, the cosine of the solar zenith angle to ξ = 0.4329, and the value of r_t immediately above cloud to 1.9 g kg^{-1}. How do changes in these parameters affect cloud lifetime? To address this, we varied these parameters one at a time and reran the simulations. The results of this sensitivity study are shown in Table 1. The cloud lifetime varies markedly when w_s varies between 1 and 6 cm s^{-1}; varies moderately when N_i varies between 1000 and 3000 m^{-3}; and varies less still when ξ varies from 0 (no solar radiation) to 1 (sun directly

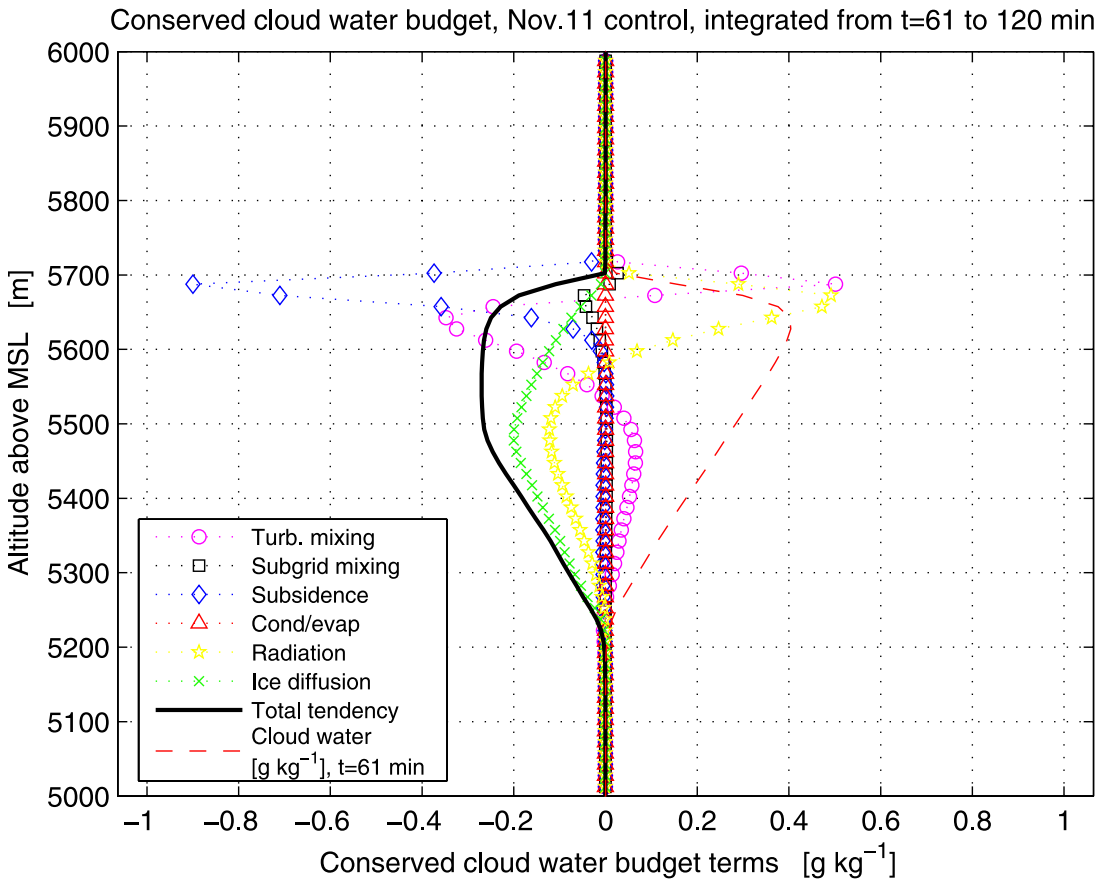

Figure 11. Budget of cloud water mixing ratio r_c derived from the conserved variables r_t and θ_l. The budget is integrated over the first simulated hour after spin-up. For reference, we plot the cloud water mixing ratio (r_c) profile at the beginning of the hour (dashed line). The total tendency (solid line) is negative, implying net depletion of cloud water, with negative (depleting) contributions from diffusional growth of ice (crosses) and large-scale subsidence (diamonds). Radiation (stars) heats and thereby depletes liquid near cloud base and cools and thereby increases liquid near cloud top. Turbulent mixing (circles) removes cloud water from midcloud and deposits it near cloud top and cloud base. Subgrid turbulent mixing (squares) is small except near cloud top. Two differences from the "raw" cloud water budget (Figure 10) are that there is now an explicit radiation term (stars) and that the condensation/evaporation term (triangles) is negligible.

overhead) or when r_t immediately above cloud varies from 1.7 to 2.1 g kg^{-1}.

[44] An increase in N_i leads to more rapid depletion of cloud because in our ice microphysics scheme, the size of a newly nucleated ice crystal is held fixed. Therefore an increase in N_i leads to an increase in ice water content and a concomitant decrease in liquid.

7.1. Equivalent Sensitivities

[45] The comparison is not general because the listed values of w_s, N_i, and so forth have been chosen somewhat arbitrarily. To remove this arbitrariness, we present "equivalent sensitivities." That is, we calculate the increment in one forcing that changes cloud lifetime as much as a given increment in another forcing. To do so, we run several simulations, each with a different value of a forcing (e.g., w_s = 1, 2, 4, 5, 6, 7, 8 cm s^{-1}) and linearly regress between forcing values and the corresponding cloud lifetimes. We estimate that increasing ξ by 1 decreases cloud lifetime as much as increasing w_s by 1.21 cm s^{-1}, increasing N_i by 781 m^{-3}, or decreasing above-cloud r_t by 0.597 g kg^{-1}. As a comparison, we linearly regress to find equivalent sensitivities for depleting liquid water path in the *first hour* of simulation after spin-up. We find that increasing ξ by 1 causes the same first-hour decrease in liquid water path as

Table 1. Sensitivity Study on Cloud Lifetime

Parameter Varied	Parameter Value	Lifetime After Spin-Up, min
Observations		74
Control run		121
Imposed subsidence velocity	6 cm s^{-1}	72
Imposed subsidence velocity	1 cm s^{-1}	277
Concentration of ice crystals	3000 m^{-3}	99
Concentration of ice crystals	1000 m^{-3}	159
Cosine of solar zenith angle	1 (overhead)	111
Cosine of solar zenith angle	0 (night)	143
Above-cloud vapor mix ratio	1.7 g kg^{-1}	111
Above-cloud vapor mix ratio	2.1 g kg^{-1}	132

increasing w_s by 3.05 cm s^{-1}, increasing N_i by 891 m^{-3}, or decreasing above-cloud r_t by 0.593 g kg^{-1}. The difference in sensitivity to w_s occurs because subsidence dominates depletion of liquid toward the end of the cloud's lifetime. Since ξ can only vary from a minimum of 0 (nighttime) to a maximum of 1 (overhead sun), these calculations show that changes in solar zenith angle have a significant effect, but that changes in w_s or N_i are at least as significant. (Recall that w_s has larger extreme values in the midtroposphere than near flat ground, where vertical velocity must tend to zero.) This occurs despite the fact that when $\xi = 1$, our simulated shortwave heating rate is substantial, with a maximum at the initial time of $\sim$1 K hr^{-1}.

[46] By definition, equivalent sensitivities are linear sensitivities. It is clear from inspection of Table 1 that the cloud sensitivities are not strictly linear. In particular, increasing w_s leads eventually to diminishing returns, because subsidence diminishes cloud most dominantly only toward the end of cloud lifetime. Nevertheless, equivalent sensitivities provide a useful rule of thumb for communicating what would otherwise require an extensive table or set of graphs.

7.2. Comments on Sensitivities to Forcings

[47] As an aside, we note that when we set $w_s = 0$, the cloud water diminishes in the first several hours, but then remains almost constant over the last 6 hours of the 11-hour simulation, despite the fact that moisture is not replenished by fluxes from the ground (not shown). This is related to the fact that as cloud top rises via entrainment, it cools adiabatically and condenses liquid [*Randall*, 1984]. It is also related to the fact that the decrease in r_t at cloud top is not large. This cloud top *decrease* can never be larger than the cloud top *value* of r_t itself, because r_t is a positive definite quantity. However, cloud top r_t is necessarily small in the cold midtroposphere (for the 11 November cloud, r_t $\sim$2.5 g kg^{-1}). Therefore air entrained into cloud top cannot have an excessive moisture deficit. These issues also arise in the study of boundary layer stratocumuli. When these clouds are overlain by dry air, they tend to dissipate after they "decouple" from below-cloud air [e.g., *Wyant and Bretherton*, 1997; *Stevens*, 2000, and references therein].

[48] The above simulation suggests that an altostratocumulus cloud may be long lived if w_s remains near zero. However, although the climatological value of w_s at any point in the atmosphere is small, w_s undergoes large temporal fluctuations at midlevels due to synoptic or mesoscale forcing. Therefore the value of w_s may significantly influence the lifetime of individual altostratocumulus clouds.

[49] Can the simulated sensitivities discussed above be reconciled with the observed diurnal cycle of altostratocumulus clouds? For instance, there is a summertime diurnal cycle of thin midlevel clouds over Oklahoma, with highest occurrence near sunrise and lowest occurrence near sunset [see *Lazarus et al.*, 2000, Figure 13]. One reasonable explanation is that solar heating evaporates cloud during the day, but not during the night, leading to maximal occurrence just before sunrise [*Lazarus et al.*, 2000]. However, our simulations seem to show that subsidence and ice are influential. Any possible diurnal effects of w_s and N_i would be masked if w_s and N_i had no correlation with time of day. Furthermore, if w_s and N_i vary little, their diurnal effects will be small. That is, the equivalent sensitivities alone cannot indicate the relative importance of solar heating versus subsidence; rather, we need to compare how much these forcings vary over a day. Clearly, ξ varies from 0 to 1. There is an observed diurnal cycle of both water vapor [*Dai et al.*, 2002, Figure 7] and vertical velocity [*Dai et al.*, 1999, Plate 1] at midaltitudes over Oklahoma. The total range of the average diurnal cycle in vertical velocity is about 1.5 cm s^{-1} at $\cong$800 hPa, and the phase of the cycle favors a midlevel cloud maximum in early morning [*Dai et al.*, 1999]. Therefore, given our equivalent sensitivities, it is likely that both subsidence and solar heating contribute to the climatological diurnal cycle of ASc. However, it is difficult to say which effect is stronger. Also, a question remains as to why there is a weak diurnal cycle over Oklahoma of thicker altostratus [*Lazarus et al.*, 2000].

8. Feedbacks Among Budget Terms

[50] We have examined four processes that affect cloud dissipation time: diffusional growth of ice, large-scale subsidence, radiative heating or cooling, and turbulent mixing. Do these processes act independently, or do they influence one another? This question can be addressed by constructing a "budget term feedback matrix." This provides a convenient overview of feedbacks among budget terms, relative to the assumption of independence or noninteraction.

8.1. Definition of Feedback Matrix and Theoretical Example

[51] We begin by integrating the "conserved" cloud water budget (equations (A4), (A5), and (A6)) for the control simulation over the entire vertical domain and a period of time. The budget can be written schematically as

$$\mathrm{Tend} = \mathrm{Ice} + \mathrm{Subs} + \mathrm{Rad} + \mathrm{Mix}, \tag{6}$$

where Tend denotes the vertically integrated time tendency of cloud water, and Ice, Subs, Rad, and Mix denote the corresponding quantities for diffusional growth of ice, large-scale subsidence, radiative heating or cooling, and turbulent mixing, respectively. Next we perturb a forcing, for instance w_s, and resimulate to obtain new perturbed budget terms:

$$\mathrm{Tend}_p = \mathrm{Ice}_p + \mathrm{Subs}_p + \mathrm{Rad}_p + \mathrm{Mix}_p. \tag{7}$$

Then we subtract the control budget (6) from the perturbed budget (7) to obtain a difference budget:

$$\Delta\mathrm{Tend} = \Delta\mathrm{Ice} + \Delta\mathrm{Subs} + \Delta\mathrm{Rad} + \Delta\mathrm{Mix}. \tag{8}$$

Finally, we divide all terms by ΔTend to obtain a normalized, dimensionless budget:

$$1 = \frac{\Delta\mathrm{Ice}}{\Delta\mathrm{Tend}} + \frac{\Delta\mathrm{Subs}}{\Delta\mathrm{Tend}} + \frac{\Delta\mathrm{Rad}}{\Delta\mathrm{Tend}} + \frac{\Delta\mathrm{Mix}}{\Delta\mathrm{Tend}}. \tag{9}$$

Each term of this normalized budget describes the change in cloud water induced by a particular process, relative to the total change in cloud water induced by all processes. All such normalized terms must sum to 1.

[52] This normalization by ΔTend discards information. For instance, the terms in equation (9) cannot tell us how changes in w_s affect ΔSubs separately from ΔTend. Therefore equation (9) cannot tell us whether ΔSubs is linearly proportional to Δw_s, or whether ΔSubs influences itself over

Adjusted Parameter	1 =	$+\frac{\Delta\text{Ice}}{\Delta\text{Tend}}$	$+\frac{\Delta\text{Subs}}{\Delta\text{Tend}}$	$+\frac{\Delta\text{Rad}}{\Delta\text{Tend}}$	$+\frac{\Delta\text{Mix}}{\Delta\text{Tend}}$
Ice number concentration: increased to 3000 m^{-3}	1 (1) =	**+1.65 (1)**	-0.37 (0)	-0.07 (0)	-0.21 (0)
Subsidence: increased to 6 cm s^{-1}	1 (1) =	-1.18 (0)	**+2.14 (1)**	+0.04 (0)	-0.001 (0)
Cos solar zenith angle (ξ): increased to 1	1 (1) =	-1.00 (0)	-0.40 (0)	**+1.89 (1)**	+0.51 (0)
Above-cloud r_t: decreased to 1.7 g kg^{-1}	1 (1) =	-1.16 (0)	+0.12 (0)	+0.23 (0)	**+1.81 (1)**

Figure 12. Feedback matrix for cloud water budget terms. The feedback matrix is the square matrix of unparenthesized numbers to the right of the column of ones. Unparenthesized values are derived from our simulations of the 11 November cloud. Values in parentheses are for the hypothetical case in which there are no interactions among budget terms. Diagonal values are in bold font for readability. Each row corresponds to a simulation in which one parameter is altered from the control simulation and set to the value indicated in the far left column. Each column of the feedback matrix corresponds to a normalized term in the budget.

time in a "temporal self-feedback." However, the normalization simplifies interpretation of both the sign and magnitude of the terms. For instance, the ratio ΔSubs/ΔTend has the same sign regardless of whether w_s is increased or decreased from the control case value. Also, magnitudes of the different terms may be directly compared to each other and the natural scale of unity because the normalization renders all terms dimensionless.

[53] How would such a budget appear if there were no interactions among terms? Suppose, for example, that the perturbed parameter is w_s, which appears only in Subs. If there are no interactions among budget terms, then Ice, Rad, and Mix do not change. Therefore the change in total cloud water tendency, ΔTend, is due entirely to ΔSubs. Then the second term on the right-hand side of equation (9) is ΔSubs/ΔTend = 1, and the other terms vanish (see "No fdbk" case in equation (10) below).

[54] Now suppose, instead, that increased subsidence diminishes ice diffusional growth, but there are no other interactions. In this case, $\Delta\text{Ice}/\Delta\text{Tend} = (\text{Ice}_p - \text{Ice})/(\text{Tend}_p - \text{Tend}) < 0$. The system now resists change, in the sense that w_s must be increased greatly to produce a small total change in cloud water tendency, ΔTend. Therefore ΔSubs/ΔTend > 1. The other terms do not interact and hence are zero. Schematically, the no-feedback and negative ice feedback budgets might be, e.g.,

$$\begin{array}{lccccccccc} \text{Eqn}: & 1 & = & \frac{\Delta\text{Ice}}{\Delta\text{Tend}} & + & \frac{\Delta\text{Subs}}{\Delta\text{Tend}} & + & \frac{\Delta\text{Rad}}{\Delta\text{Tend}} & + & \frac{\Delta\text{Mix}}{\Delta\text{Tend}} \\ \text{No fdbk}: & 1 & = & 0 & + & 1 & + & 0 & + & 0 \\ \text{Neg fdbk}: & 1 & = & -0.5 & + & 1.5 & + & 0 & + & 0. \end{array} \quad (10)$$

8.2. Feedback Matrix for the 11 November Cloud

[55] Armed with this background intuition, we proceed to perturb a forcing parameter associated with one of the four terms (processes) and rerun the simulation. We repeat for each of the other three terms and corresponding parameters. Specifically, for the first term, we increase N_i to 3000 m^{-3}; for the second, we increase w_s to 6 cm s^{-1}; for the third, we increase ξ to 1; and for the fourth, we decrease above-cloud r_t to 1.7 g kg^{-1}. Using each perturbed simulation, we compute the terms in the normalized budget equation (9), yielding a total of four equations. We arrange the right-hand side of these equations in a square "budget term feedback matrix," **F**, shown in Figure 12. The first row in the matrix corresponds to the first sensitivity simulation (N_i = 3000 m^{-3}), and so forth for the other rows. Not included in the definition of the feedback matrix is the left-hand column of the table, which contains all ones.

[56] The diagonal elements (written in boldface font) represent the normalized change in a budget term (e.g., Subs) when there is a change in the same term's forcing parameter (e.g., w_s). The off-diagonal elements indicate how a change in one term's forcing parameter (e.g., w_s) influences another budget term (e.g., Ice). Each row of the feedback matrix must sum to one (rounding errors prevent exact agreement in the presented numbers). When there are no interactions, the feedback matrix is the identity matrix. The elements of this noninteraction matrix, i.e., the identity matrix, are listed in Figure 12 in parentheses. The elements not enclosed in parentheses are results from our 11 November simulations. Comparing the two sets of numbers is revealing.

[57] Let us first interpret the sign of the off-diagonal elements. Consider the element in the 2nd row and 1st column, $\mathbf{F}_{21} = -1.18$. This corresponds to the change in Ice tendency (1st column) when w_s is increased (2nd row). It is

negative. This negative sign means that Ice resists the change in Tend induced by the change in w_s. Why is this? Diffusional growth of ice crystals falling through cloud depletes more liquid when the liquid layer is vertically extensive. Suppose, then, that w_s is increased. The increased subsidence thins the cloud layer more rapidly, rendering $\Delta\text{Tend} = (\text{Tend}_p - \text{Tend}) < 0$. Then ice diffusional growth, acting on the thinned cloud, no longer depletes liquid so rapidly, rendering $\Delta\text{Ice} = (\text{Ice}_p - \text{Ice}) > 0$. Since ΔIce and ΔTend have opposite sign, $\mathbf{F}_{21}$ is negative. In contrast, if subsidence and ice diffusional growth were independent, $\mathbf{F}_{21}$ would be zero.

[58] The off-diagonal elements in the Ice (1st) column ($\mathbf{F}_{21}$, $\mathbf{F}_{31}$, $\mathbf{F}_{41}$) are negative. This implies that, in our simulations, ice diffusional growth acts as a negative feedback.

[59] The matrix also reveals positive feedbacks, the largest of which is $\mathbf{F}_{34} = 0.51$. This element indicates that if solar heating increases and thereby depletes liquid faster, turbulent mixing acts in the same direction. In our simulations, the mechanism appears to be as follows. Increased solar heating diminishes turbulence, which then causes less low-θ_l air to be mixed upward through cloud base. The less intense turbulent cooling then leads to faster depletion of cloud water, a positive feedback (not shown). Other off-diagonal elements indicate weaker positive or negative feedbacks.

[60] Now consider the diagonal elements. For instance, the element $\mathbf{F}_{22}$ (row w_s, column Subs) exceeds 1, the corresponding value for the identity matrix. How should we interpret this? All elements of each row must sum to unity. If the sum of the off-diagonal elements of a row is negative, then the diagonal element must exceed 1. The fact that $\mathbf{F}_{22} > 1$ means that the effect of a change in w_s on liquid is opposed, on average, by the other processes. In $\mathbf{F}$, all the diagonal elements exceed 1. This implies that each of our perturbations is subjected to a net negative feedback; that is, when one process changes cloud water, the net effect of all other processes is to resist this change. This net negative feedback is dominated by that associated with diffusional growth of ice.

8.3. Comparison With Standard Feedback Analysis

[61] There are several differences between our feedback matrix and a standard feedback analysis [e.g., *Stephens* 2005]. To perform a standard feedback analysis, one chooses a control parameter whose value may be varied between simulations. Subsequently, one performs a control simulation and then compares two perturbed simulations, one in which certain physical processes are shut off and one in which they are turned on. For instance, to assess a global climate feedback, one may double the mixing ratio of carbon dioxide, and compare the simulated climatological temperature change that occurs when processes that alter water vapor mixing ratio are either shut off or turned on. In contrast, our analysis involves control parameters such as w_s, and control and perturbed simulations, but none of our simulations attempts to shut off any processes. Our feedback matrix elements include the effects of all processes acting simultaneously. Therefore we cannot compute traditionally defined feedback parameters. Nevertheless, we still obtain information about separate processes because we compute each separate budget term.

[62] Another difference from the standard feedback analysis is that it is difficult for a standard feedback analysis to analyze a complete but nonoverlapping set of processes. For instance, it is difficult to formulate a complete but distinct set of feedbacks that affect global temperature, such as the water vapor feedback, cloud feedbacks, and so forth. In contrast, our feedback matrix is "complete" in the sense that it estimates all budget terms that deplete cloud water. However, it is incomplete in the sense that it only lists changes in budget *terms*, not prognostic *variables* such as temperature, moisture, and so forth.

9. Conclusions

[63] This paper analyzes the dissipation of an altostratocumulus (ASc) cloud that was observed on 11 November 1999. Our goal is to investigate how dissipation time is affected by the four main physical processes: diffusional growth of ice, large-scale subsidence, radiation, and turbulent mixing. Our main tool of inquiry is numerical simulations. We have applied two main diagnostics.

[64] The first diagnostic is a budget equation of cloud water (equations (A4), (A5), and (A6)). This allows us to compare, side by side, how the four processes affect cloud water (Figure 11). The major assumptions of our budget are that the cloud is overcast (i.e., has cloud fraction of 1), and that the cloud is saturated with respect to liquid. We find that subsidence and ice diffusional growth are nonpositive at all altitudes. In our particular simulations, this leads to strong net depletion of liquid. Radiation and turbulent mixing have smaller net effects because each partially self-cancels in the vertical.

[65] The second diagnostic is a "budget term feedback matrix." This is constructed from the budget equation for cloud water and shows how changes in one budget term affect another. Negative *off-diagonal* elements indicate that there is a negative feedback; that is, a change in cloud water tendency induced by one process is opposed or resisted by another process. The opposite is true for positive off-diagonal elements. A *diagonal* element exceeds 1 if there is a net negative feedback by all other processes, i.e., if one process' effect on cloud water is opposed by the net effect of all other processes. In our particular simulations, the diffusional growth of ice is a negative feedback. This is because if one process reduces cloud layer thickness, then ice depletes liquid less effectively. The budget term feedback matrix provides a broad overview of feedbacks. It may prove useful for a variety of problems.

[66] We also document the relative effectiveness of physical processes in shortening cloud lifetime via equivalent sensitivities. These are obtained by performing sensitivity studies and linearly regressing on cloud lifetime. We estimate that, for our case, increasing the cosine of the solar zenith angle ξ by 1 (the maximum possible change) curtails cloud lifetime by the same amount as increasing subsidence velocity w_s by 1.21 cm s^{-1}, increasing ice number concentration by 781 m^{-3}, or decreasing above-cloud r_t by 0.597 g kg^{-1}.

[67] *Lazarus et al.* [2000] observed that thin midlevel clouds have a diurnal cycle over Oklahoma and hypothe-

sized that this is due to the diurnal cycle of solar radiation. Asserting that solar radiation is a significant factor is consistent with the simulations of *Liu* [1998] and our own. However, it is also plausible that the diurnal cycle of large-scale vertical velocity [*Dai et al.*, 1999] contributes significantly, given our simulations' sensitivity of cloud lifetime to subsidence velocity.

[68] Finally, we add the caveat that our results are derived from a single case study. Clearly, there exists a wide variety of altostratocumulus, and our numbers cannot be assumed to have general applicability. In particular, some altostratocumulus clouds glaciate rapidly, but others contain no ice. This influences the strength of the ice feedback. Further study is desirable on the 11 November case and other cases using a more sophisticated ice microphysical scheme.

Appendix A: Cloud Water Budget Derived From Conserved Variables

[69] To write our budget for liquid, we first introduce a variable, s, that equals cloud water mixing ratio, r_c, when it is positive, but also can be negative. Specifically, $r_c = s\,H(s)$ [*Larson*, 2004], where $H(s)$ is the Heaviside step function, which is 0 when $s < 0$ and 1 when $s > 1$. We use the following equation to relate s and the quantity we want, the time tendency of the horizontal average of r_c, $\langle r_c \rangle$:

$$\begin{aligned}\frac{\partial}{\partial t}\langle r_c\rangle &= \frac{\partial}{\partial t}\langle sH(s)\rangle \\ &= \left\langle \frac{\partial}{\partial t}[sH(s)] \right\rangle \\ &= \left\langle \underbrace{s\frac{\partial H(s)}{\partial t}}_{\text{neglect}} + H(s)\frac{\partial s}{\partial t} \right\rangle \\ &= \left\langle H(s)\frac{\partial s}{\partial t} \right\rangle.\end{aligned} \tag{A1}$$

The second equality follows because we may interchange a fixed spatial integration and a time derivative. The third equality follows by the product rule of calculus. The fourth equality involves dropping a product of two factors, one of which is nonzero only at cloud edge ($\partial H(s)/\partial t$), and one of which is zero at cloud edge (s).

[70] After relating r_c and s, the key to our budget derivation is to write s in terms of the conserved variables liquid water potential temperature, θ_l, and total water mixing ratio (vapor + liquid), r_t:

$$\frac{\partial s}{\partial t} = \left(\frac{\partial s}{\partial \theta_l}\right)_{r_t,p}\frac{\partial \theta_l}{\partial t} + \left(\frac{\partial s}{\partial r_t}\right)_{\theta_l,p}\frac{\partial r_t}{\partial t} + \left(\frac{\partial s}{\partial p}\right)_{\theta_l,r_t}\frac{\partial p}{\partial t}. \tag{A2}$$

Here p denotes pressure and t denotes time. This equality requires the assumption that there is no vapor supersaturation anywhere, and no subsaturation in the presence of liquid. The partial derivatives $\left(\frac{\partial s}{\partial \theta_l}\right)_{r_t,p}$, $\left(\frac{\partial s}{\partial r_t}\right)_{\theta_l,p}$, and $\left(\frac{\partial s}{\partial p}\right)_{\theta_l,r_t}$ are given in *Larson* [2004]. For our case we may set $\frac{\partial p}{\partial t} = 0$.

[71] Now we multiply our budget equation (A2) by $H(s)$ and average horizontally. We find terms such as $\langle H(s)f\rangle$, which is the within-cloud contribution of an arbitrary term f. Since we know the grid box average source, but not the within-cloud source, we approximate

$$\langle H(s)f\rangle \cong \langle H(s)\rangle\langle f\rangle = C\langle f\rangle, \tag{A3}$$

where $C = \langle H(s)\rangle$ is cloud fraction. Equation (A3) is not highly accurate for partly cloudy regions, and we do not recommend its general use. However, in our overcast case, it is sufficient. Including the prefactor of C does yield more accurate results near cloud top, where the horizontally averaged cloud fraction is between 0 and 1. However, the approximation may not be sufficiently accurate for stratocumulus cases with large variations in moisture and temperature near cloud top.

[72] Combining equations (A1) and (A2), averaging over the horizontal, and using equation (A3), we find

$$\begin{aligned}\frac{\partial}{\partial t}\langle r_c\rangle &\cong C\left\langle \left(\frac{\partial s}{\partial \theta_l}\right)_{r_t,p}\frac{\partial \theta_l}{\partial t}\right\rangle + C\left\langle \left(\frac{\partial s}{\partial r_t}\right)_{\theta_l,p}\frac{\partial r_t}{\partial t}\right\rangle \\ &\cong C\left\langle \left(\frac{\partial s}{\partial \theta_l}\right)_{r_t,p}\right\rangle\left\langle \frac{\partial \theta_l}{\partial t}\right\rangle + C\left\langle \left(\frac{\partial s}{\partial r_t}\right)_{\theta_l,p}\right\rangle\left\langle \frac{\partial r_t}{\partial t}\right\rangle.\end{aligned} \tag{A4}$$

We assume that θ_l and r_t obey the following advection-diffusion equations, which can be written schematically as

$$\left\langle \frac{\partial \theta_l}{\partial t}\right\rangle = \mathrm{Ice}_{\theta_l} + \mathrm{Subs}_{\theta_l} + \mathrm{Rad}_{\theta_l} + \mathrm{Mix}_{\theta_l} \tag{A5}$$

and

$$\left\langle \frac{\partial r_t}{\partial t}\right\rangle = \mathrm{Ice}_{r_t} + \mathrm{Subs}_{r_t} + \mathrm{Mix}_{r_t}. \tag{A6}$$

These budget equations are embedded in our LES code [*Golaz et al.*, 2005]. Combining equation (A4) with equations (A5) and (A6) yields the final budget of cloud water. Integrating over time and the vertical direction yields equation (6).

[73] **Acknowledgments.** V. E. Larson, A. J. Smith, M. J. Falk, and Kurt Kotenberg are grateful for financial support provided by grant ATM-0239982 from the National Science Foundation and by subaward G-7424-1 from the DoD Center for Geosciences/Atmospheric Research at Colorado State University via Cooperative Agreement DAAD19-02-2-0005 with the Army Research Laboratory. A portion of this research was performed while J.-C. Golaz held a National Research Council Research Associateship Award at the Naval Research Laboratory, Monterey, California. COAMPS® is a registered trademark of the Naval Research Laboratory.

References

Bott, A. (1989), A positive definite advection scheme obtained by nonlinear renormalization of the advective fluxes, *Mon. Weather Rev.*, *117*, 1006–1015.

Brown, A. R., et al. (2002), Large-eddy simulation of the diurnal cycle of shallow cumulus convection overland, *Q. J. R. Meteorol. Soc.*, *128*, 1075–1093.

Clark, P. D., T. W. Choularton, P. R. A. Brown, P. R. Field, A. J. Illingworth, and R. J. Hogan (2005), Numerical modelling of mixed-phase frontal clouds observed during the CWVC project, *Q. J. R. Meteorol. Soc.*, *131*, 1677–1693.

Dai, A., F. Giorgi, and K. E. Trenberth (1999), Observed and model-simulated diurnal cycles of precipitation over the contiguous United States, *J. Geophys. Res.*, *104*, 6377–6402.

Dai, A., J. Wang, R. H. Ware, and T. Van Hove (2002), Diurnal variation in water vapor over North America and its implications for sampling errors

in radiosonde humidity, *J. Geophys. Res.*, *107*(D10), 4090, doi:10.1029/2001JD000642.
Deardorff, J. W. (1980), Stratocumulus-capped mixed layers derived from a three-dimensional model, *Boundary Layer Meteorol.*, *18*, 495–527.
Duynkerke, P. G., et al. (2004), Observations and numerical simulations of the diurnal cycle of the EUROCS stratocumulus case, *Q. J. R. Meteorol. Soc.*, *130*, 3269–3296.
Fleishauer, R. P., V. E. Larson, and T. H. Vonder Haar (2002), Observed microphysical structure of midlevel, mixed-phase clouds, *J. Atmos. Sci.*, *59*, 1779–1804.
Gedzelman, S. D. (1988), In praise of altocumulus, *Weatherwise*, *41*, 143–149.
Golaz, J.-C., S. Wang, J. D. Doyle, and J. M. Schmidt (2005), Second and third moment vertical velocity budgets derived from COAMPS-LES, *Boundary Layer Meteorol.*, *116*, 487–517.
Gu, Y., and K.-N. Liou (2000), Interactions of radiation, microphysics, and turbulence in the evolution of cirrus clouds, *J. Atmos. Sci.*, *57*, 2463–2479.
Hodur, R. M. (1997), The Naval Research Laboratory's Coupled Ocean/Atmosphere Mesoscale Prediction System (COAMPS), *Mon. Weather Rev.*, *125*, 1414–1430.
Katzfey, J. J., and B. F. Ryan (2000), Midlatitude frontal clouds: GCM-scale modeling implications, *J. Clim.*, *13*, 2729–2745.
Kogan, Z. N., Y. L. Kogan, and D. Mechem (2001), The statistical formulations of cloud inhomegeneity parameters over the southern great plains, paper presented at Eleventh ARM Science Team Meeting, Atmos. Radiat. Meas. Program, Dep. of Energy, Atlanta, Ga.
Köhler, M. (1999), Explicit prediction of ice clouds in general circulation models, Ph.D. thesis, 167 pp., Univ. of Calif., Los Angeles.
Larson, V. E. (2004), Prognostic equations for cloud fraction and liquid water, and their relation to filtered density functions, *J. Atmos. Sci.*, *61*, 338–351.
Larson, V. E., R. P. Fleishauer, J. A. Kankiewicz, D. L. Reinke, and T. H. Vonder Haar (2001), The death of an altocumulus cloud, *Geophys. Res. Lett.*, *28*, 2609–2612.
Larson, V. E., K. E. Kotenberg, and N. B. Wood (2006), An analytic longwave radiation formula for liquid layer clouds, *Mon. Weather Rev.*, in press.
Lazarus, S. M., S. K. Krueger, and G. G. Mace (2000), A cloud climatology of the Southern Great Plains ARM CART, *J. Clim.*, *13*, 1762–1775.
Liu, S. (1998), Numerical modeling of altocumulus cloud layers, Ph.D. thesis, 147 pp., Univ. of Utah, Salt Lake City.
Liu, S., and S. K. Krueger (1998), Numerical simulations of altocumulus using a cloud resolving model and a mixed layer model, *Atmos. Res.*, *47–48*, 461–474.
Mitchell, D. L. (1996), Use of mass- and area-dimensional power laws for determining precipitation particle terminal velocities, *J. Atmos. Sci.*, *53*, 1710–1723.
Poellot, M. R., W. P. Arnott, and J. Hallett (1999), In-situ observations of contrail microphysics and implications for their radiative impact, *J. Geophys. Res.*, *104*, 12,077–12,084.
Pruppacher, H. R., and J. D. Klett (1997), *Microphysics of Clouds and Precipitation*, 2nd ed., 954 pp., Springer, New York.
Randall, D. A. (1984), Stratocumulus cloud deepening through entrainment, *Tellus, Ser. A*, *36*, 446–457.
Rogers, R. R., and M. K. Yau (1989), *A Short Course in Cloud Physics*, 3rd ed., 290 pp., Elsevier, New York.
Rutledge, S. A., and P. V. Hobbs (1983), The mesoscale and microscale structure of organization of clouds and precipitation in midlatitude cyclones: VIII: A model for the "seeder-feeder" process in warm-frontal rainbands, *J. Atmos. Sci.*, *40*, 1185–1206.
Ryan, B. F., et al. (2000), Simulations of a cold front by cloud-resolving, limited-area, and large-scale models, and a model evaluation using in situ and satellite observations, *Mon. Weather. Rev.*, *128*, 3218–3235.
Shettle, E. P., and J. A. Weinman (1970), The transfer of solar irradiance through inhomogeneous turbid atmospheres evaluated by Eddington's approximation, *J. Atmos. Sci.*, *27*, 1048–1055.
Starr, D. O., and S. K. Cox (1985), Cirrus clouds. part II: Numerical experiments on the formation and maintenance of cirrus, *J. Atmos. Sci.*, *42*, 2682–2694.
Stephens, G. L. (2005), Cloud feedbacks in the climate system: A critical review, *J. Clim.*, *18*, 237–273.
Stephens, G. L., P. M. Gabriel, and P. T. Partain (2001), Parameterization of atmospheric radiative transfer. part I: Validity of simple models, *J. Atmos. Sci.*, *58*, 3391–3409.
Stephens, G. L., N. Wood, and P. Gabriel (2004), An assessment of the parameterization of subgrid-scale cloud effects on radiative transfer. part I: Vertical overlap, *J. Atmos. Sci.*, *61*, 715–732.
Stevens, B. (2000), Cloud transitions and decoupling in shear-free stratocumulus-topped boundary layers, *Geophys. Res. Lett.*, *27*, 2557–2560.
Stevens, B., et al. (2001), Simulations of trade wind cumuli under a strong inversion, *J. Atmos. Sci.*, *58*, 1870–1891.
Stevens, B., et al. (2005), Evaluation of large-eddy simulations via observations of nocturnal marine stratocumulus, *Mon. Weather Rev.*, *133*, 1443–1462.
Stull, R. B. (1988), *An Introduction to Boundary Layer Meteorology*, 666 pp., Springer, New York.
Vonder Haar, T. H., et al. (1997), Overview and objectives of the DoD Center for Geosciences sponsored "Complex Layered-Cloud Experiment", paper presented at Cloud Impacts on DoD Operations and Systems Conference, Phillips Lab., Newport, R. I.
Wang, S., and Q. Wang (1999), On condensation and evaporation in turbulence cloud parameterizations, *J. Atmos. Sci.*, *56*, 3338–3344.
Wang, S., Q. Wang, and G. Feingold (2003), Turbulence, condensation, and liquid water transport in numerically simulated nonprecipitating stratocumulus clouds, *J. Atmos. Sci.*, *60*, 262–278.
Weaver, C. P., J. R. Norris, N. D. Gordon, and S. A. Klein (2005), Dynamical controls on sub-global climate model grid-scale cloud variability for Atmospheric Radiation Measurement Program (ARM) case 4, *J. Geophys. Res.*, *110*, D15S05, doi:10.1029/2004JD005022.
Wyant, M. C., and C. S. Bretherton (1997), Numerical simulations and a conceptual model of the stratocumulus to trade cumulus transition, *J. Atmos. Sci.*, *54*, 168–192.
Xu, K.-M., et al. (2005), Modeling springtime shallow frontal clouds with cloud-resolving and single-column models, *J. Geophys. Res.*, *110*, D15S04, doi:10.1029/2004JD005153.
Zhang, M. H., et al. (2005), Comparing clouds and their seasonal variations in 10 atmospheric general circulation models with satellite measurements, *J. Geophys. Res.*, *110*, D15S02, doi:10.1029/2004JD005021.

M. J. Falk, K. E. Kotenberg, V. E. Larson, and A. J. Smith, Atmospheric Science Group, Department of Mathematical Sciences, University of Wisconsin-Milwaukee, P.O. Box 413, Milwaukee, WI 53201-0413, USA.
J.-C. Golaz, UCAR Visiting Scientist Program, NOAA GFDL, Princeton University, Forrestal Campus, P.O. Box 308, Princeton, NJ 08542, USA.